Phytochemistry 251 (2026) 115010

Contents lists available at ScienceDirect

Phytochemistry

journal homepage: www.elsevier.com/locate/phytochem

Antiviral amide derivatives from *Uvaria siamensis*

Bastien Petit [a], Thibaud Goupil [b], Linh Hoang Phan [a], Charline Herrscher [b], Thomas Gaslonde [c], Xavier Cachet [c], Van Cuong Pham [d], Thi Mai Huong Doan [d], Karin Séron [e], Fanny Roussi [a], Sandy Desrat [a], Marc Litaudon [a,*], Chaker El Kalamouni [b,**], Cécile Apel [a,***]

[a] Université Paris-Saclay, CNRS, Institut de Chimie des Substances Naturelles, UPR 2301, Gif-sur-Yvette, 91198, France
[b] Unité Mixte Processus Infectieux en Milieu Insulaire Tropical, Université de La Réunion, INSERM U1187, CNRS UMR 9192, IRD UMR 249, Plateforme Technologique CYROI, Sainte Clotilde, 97491, France
[c] Université Paris-Cité, CNRS, UMR 8038 CiTCoM, Faculté de Pharmacie de Paris, Paris, 75006, France
[d] Institute of Chemistry, Vietnam Academy of Science and Technology (VAST), 18 Hoang Quoc Viet, Nghia Do, Hanoi, 10072, Viet Nam
[e] Center for Infection and Immunity of Lille (CIIL), Institut Pasteur de Lille, Université de Lille, INSERM U1019, CNRS UMR 8204, CHU Lille, Lille, 59000, France

ARTICLE INFO

Keywords:
Uvaria siamensis
Annonaceae
Toussaintine
Melodamide
Antiviral agents
HCoV-229E
SARS-CoV-2

ABSTRACT

A screening of 824 plant extracts from Rutaceae and Annonaceae species against a human alphacoronavirus (HCoV-229E-Luc) identified *Uvaria siamensis* (Scheff.) L.L.Zhou, Y·C·F.Su & R.M.K.Saunders (Annonaceae) as a promising source of bioactive metabolites. Subsequent bioassay-guided fractionation of its ethyl acetate and methanol leaf extracts led to the isolation of three previously undescribed amide derivatives, melodamides B–D (**3**–**5**), together with melodamide A (**2**), uvariadiamide (**6**), (+)- and (−)-toussaintine C (**1**), and five known polyphenols (**7**–**11**). The structures of compounds **1**–**11** were characterized by comprehensive spectroscopic analysis and comparison with literature data. In HCoV-229E-infected Huh-7 cells, (+)-toussaintine C (**1**) and melodamide C (**4**) were the most potent metabolites, with IC_{50} values of 1.4 and 1.8 μM and selectivity indices of 43 and 39, respectively, while melodamide A (**2**) also displayed notable activity, with an IC_{50} of 4.2 μM and an SI of 11. In contrast, polyphenols **7**–**11** displayed weaker antiviral effects restricted to the low- to mid-micromolar range. Extension of the profiling to a pandemic clinical isolate of SARS-CoV-2 in Vero cells, showed that both enantiomers of toussaintine C, as well as melodamides A and C, retained measurable inhibition in the mid-micromolar range, whereas most polyphenols lost activity. Taken together, these results identify amide derivatives from *U. siamensis* as antiviral scaffolds with preferential activity against an alphacoronavirus model, and highlight this species as a valuable source of small-molecule coronavirus inhibitors.

1. Introduction

Emerging and re-emerging viral diseases continue to represent a major and unpredictable threat to global health. Among them, coronaviruses have repeatedly crossed the species barrier over the past two decades, giving rise to severe outbreaks such as SARS (2002–2003), MERS (2012), and most recently COVID-19 (de Wit et al., 2016). These events have highlighted the remarkable evolutionary plasticity of coronaviruses, which allows rapid adaptation through mutations and recombination within diverse animal reservoirs. Beyond the immediate impact of each epidemic, they underscore the need for sustained antiviral preparedness targeting conserved viral and host pathways. Despite the accelerated development of vaccines and therapeutic antibodies, effective small-molecule antivirals against coronaviruses remain scarce and largely limited to polymerase or protease inhibitors developed in the context of SARS-CoV-2 (Kronenberger et al., 2023). Identifying previously unreported scaffolds capable of interfering with coronavirus replication, ideally by targeting host factors or alternative viral proteins, therefore remains a critical challenge for future pandemic response.

To identify natural antiviral scaffolds, a screening program of tropical plant extracts was established using the human alphacoronavirus

* Corresponding author.
** Corresponding author.
*** Corresponding author.
E-mail addresses: marc.litaudon91@gmail.com (M. Litaudon), chaker.el-kalamouni@univ-reunion.fr (C.E. Kalamouni), cecile.apel@cnrs.fr (C. Apel).

https://doi.org/10.1016/j.phytochem.2026.115010
Received 18 December 2025; Received in revised form 26 June 2026; Accepted 28 June 2026
Available online 29 June 2026

HCoV-229E as a biosafe model of coronavirus infection. This model provides a robust platform for assessing inhibitors of viral entry and replication under BSL-2 conditions (Chambon et al., 2023; Petit et al., 2024; Sukumaran et al., 2024). A collection of 824 plant extracts from Rutaceae and Annonaceae species was established and detailed in previous reports (Petit et al., 2024; Sukumaran et al., 2024; Apel et al., 2025). At a test concentration of 25 μg mL^{-1}, approximately 6% of the evaluated extracts were considered active, exhibiting at least 80% inhibition of viral infection compared to untreated infected cells. Among the most promising candidates, the ethyl acetate (EtOAc) and methanol (MeOH) extracts obtained from the leaves of *Uvaria siamensis* (Scheff.) L. L.Zhou, Y·C·F.Su & R.M.K.Saunders (Annonaceae), were selected for further phytochemical and antiviral investigation.

This species, formerly *Melodorum fruticosum* Lour. (Turner, 2018), is a woody climber or shrub with fragrant pale-yellow flowers and ovoid yellow fruits, native to Southeast Asia and valued for its aromatic flowers and traditional medicinal uses (Zhou et al., 2009). It was reported to contain a variety of bioactive compounds. For example, root-derived lanostane triterpenes and chalcones exhibited cytotoxic, antitumor, and antiplasmodial activities, while flower-derived γ-alkylidenebutenolides, other furanone derivatives and phenolic amides showed antioxidant, antifungal, anti-melanogenic, and anti-inflammatory properties (Pripdeevech and Chukeatirote, 2010; Chan et al., 2013; Salae et al., 2017; Schevenels et al., 2025; Tabtimmai et al., 2025; Takashima et al., 2025). Flavonoids and heptenes isolated from the stem bark were also reported to display α-glucosidase inhibitory and cytotoxic activities (Jung et al., 1990, 1991; Do and Sichaem, 2022; Nguyen et al., 2024).

This study presents a bioassay-guided phytochemical investigation of the leaves of *U. siamensis* together with the antiviral evaluation of the resulting metabolites against HCoV-229E and SARS-CoV-2 infection models.

2. Results and discussion

Biological screening of part of a plant extract collection, comprising Annonaceae and Rutaceae species from Malaysia, Vietnam, and New Caledonia, was performed against HCoV-229E using Huh-7 and Huh-7-TMPRSS2 cells infected with a recombinant luciferase-expressing clone (HCoV-229E-Luc) (Chambon et al., 2023; Petit et al., 2024). This screening identified the EtOAc leaf extract of the Vietnamese species *U. siamensis* as particularly active, reducing viral infection to 1% and 5% relative to the DMSO-treated control (100% infection) at concentrations of 25 and 10 μg mL^{-1}, respectively. The EtOAc extract displayed a half-maximal inhibitory concentration (IC_{50}) of 0.33 μg mL^{-1}, while the subsequent methanol (MeOH) extract also retained strong antiviral activity with an IC_{50} of 0.13 μg mL^{-1}, justifying its fractionation for further phytochemical investigation. Bioassay-guided fractionation of both extracts was subsequently performed on the HCoV-229E/Huh-7 model, with systematic evaluation of cytotoxicity and antiviral efficacy at each purification step to ensure the selection of genuinely active, non-toxic fractions. This strategy led to the isolation of eleven compounds belonging to two distinct chemical families: amide derivatives and polyphenolic compounds (Fig. 1).

2.1. Structure elucidation

Compound **1** was identified as toussaintine C based on NMR spectroscopic analysis and comparison with literature data (Samwel et al., 2011; Zhou et al., 2023). Toussaintine C was first reported in 2011 by Samwel et al. as a constituent of the leaf extract of *Toussaintia orientalis*. It was later isolated in 2019 by Jaidee et al. from the dried fruits of *Melodorum siamensis*, which likely corresponds to *Melodorum siamense* (Scheff.) Bân, a synonym of *U. siamensis*, the species investigated in the present study (Turner, 2018). Compound **1** was obtained as a racemic mixture, as indicated by an optical rotation value of zero. Its ^1H NMR spectrum displayed duplicated resonances, consistent with the observations of Zhou et al. (2023), and attributable to the partial double-bond character of the C–N bond in the *N*-cinnamoylindolidinoid moiety, which restricts bond rotation. High-temperature NMR experiments also confirmed this interpretation by showing coalescence of the duplicated signals, in agreement with the data of Zhou et al. (2023). In addition,

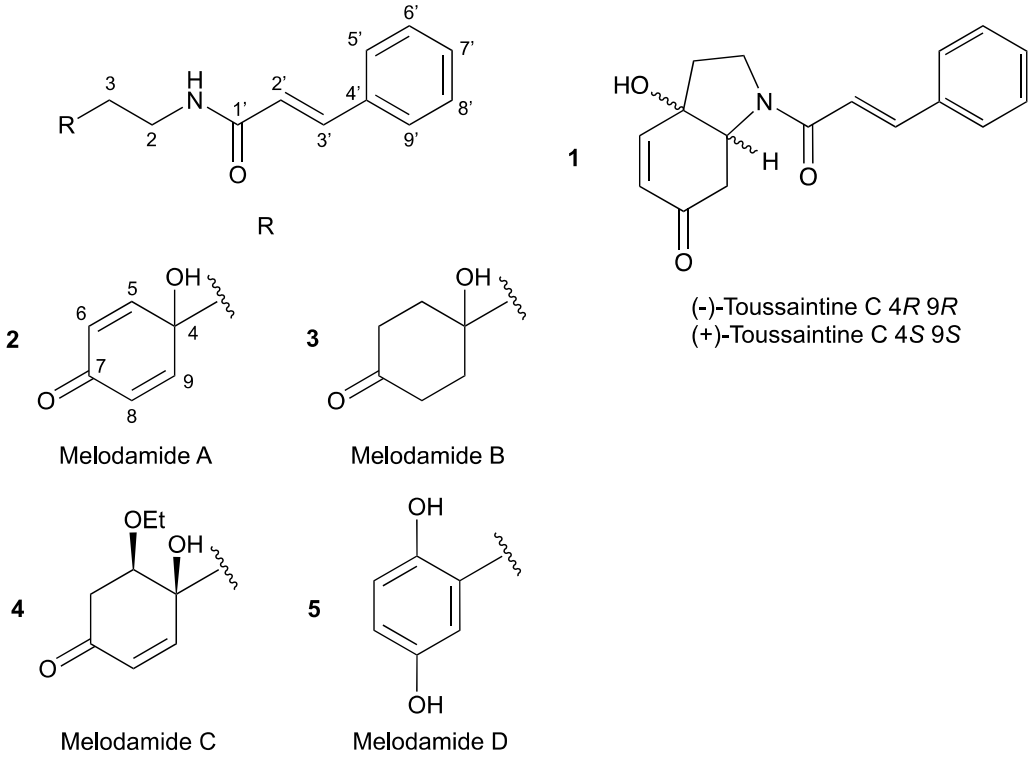

Fig. 1. Structures of compounds **1**–**5**.

single-crystal X-ray diffraction analysis of a racemic crystal confirmed the structure and established the relative configuration of compound **1**. Resolution of compound **1** by semipreparative chiral-phase HPLC afforded (+)- and (−)-toussaintine C. Their optical rotation values were compared with those reported by Jaidee et al. (2019), showing similar magnitudes and opposite signs, which allowed the assignment of (+)-**1** as (4*S*,9*S*)-toussaintine C and (−)-**1** as (4*R*,9*R*) toussaintine C.

Compound **2** was identified as the known melodamide A by comparison of its spectroscopic data with literature values (Chan et al., 2013). Partial conversion of melodamide A into toussaintine C was observed during purification and NMR analysis under mildly acidic conditions, suggesting that melodamide A may act as a biosynthetic precursor of toussaintine C. This acid-mediated transformation may influence the relative abundance of toussaintine C in isolated fractions.

Compound **3** was obtained as a yellow amorphous solid. Its HRESIMS data showed a $[M + H]^+$ ion peak at *m/z* 288.1592 (calcd for $C_{17}H_{22}NO_3^+$ 288.1594) corresponding to the molecular formula $C_{17}H_{21}NO_3$ and indicating eight degrees of unsaturation (Fig. S1). The UV spectrum of **3** showed absorption maxima at 274 and 216 nm, while the IR spectrum displayed characteristic bands for a hydroxy group (3318 cm $^{-1}$), a carbonyl function (1707 cm^{-1}), and an amide functionality (1656 cm^{-1}). The NMR spectroscopic data of compound **3** showed similar structural features to those of melodamide A (Fig. S2–S6, Table 1). In particular, the presence of a cinnamoyl-derived spin system was evident from the characteristic *trans*-olefinic protons and aromatic resonances. The *N*-ethylcinnamamide moiety was established on the basis of key 2D correlations (Chan et al., 2013). The ^{1}H NMR spectrum displayed an amide proton resonance at δ_H 6.18 (1H, br s, NH), a series of five aromatic protons at δ_H 7.50 (2H, m, H-5′, H-9′), 7.39 (2H, m, H-6′, H-8′) and 7.38 (1H, m, H-7′), *trans*-olefinic signals at δ_H 7.66 (1H, d, J = 15.5 Hz, H-3′) and 6.38 (1H, d, J = 15.5 Hz, H-2′), and upfield resonances for four coupled protons at δ_H 3.62 (2H, q, J = 6.0 Hz, H-2) and 1.84 (2H, t, J = 6.0 Hz, H-3). Compound **3** differed from melodamide A by displaying two pairs of methylene resonances at δ_H 2.10/1.79 (4H, H_2-5, H_2-9) and 2.77/2.26 (4H, H_2-6, H_2-8), in place of the four conjugated olefinic protons characteristic of melodamide A. This suggested reduction of the $\Delta^{5,6}$ and $\Delta^{8,9}$ double bonds of the *p*-quinol moiety of melodamide A into methylene groups. The *N*-(ethyl)hydroxycyclohexanone moiety was established on the basis of key COSY correlations between the amide proton and the methylene protons H_2-2 and H_2-3, as well as between H_2-5/H_2-6 and H_2-9/H_2-8 (Fig. 2). Additional HMBC correlations supported this assignment, including cross-peaks from H_2-2 to the carbonyl carbon at δ_C 166.9 (C-1'), the methylene carbon C-3 (δ_C 41.9), and the oxygenated tertiary carbon at δ_C 69.6 (C-4). Further HMBC correlations from H_2-3 to C-4 and C-5/C-9 (δ_C 41.9), from H_2-5/H_2-9 (δ_H 1.79) to C-6/C-8 (δ_C 37.1), and from H_2-6/H_2-8 (δ_H 2.77) to both C-5/C-9 and the carbonyl C-7 (δ_C 211.6) confirmed the overall structure of compound **3**, designated as melodamide B (Fig. 2).

Compound **4** was isolated as a yellow solid. Its molecular formula, $C_{19}H_{23}NO_4$, was established from HRESIMS data, which exhibited a $[M + H]^+$ ion peak at *m/z* 330.1710 (calcd for $C_{19}H_{24}NO_4^+$ 330.1700) (Fig. S7), consistent with nine degrees of unsaturation. NMR spectroscopic analysis revealed the presence of the same *N*-ethylcinnamamide moiety as in melodamides A and B (Fig. S8–S13). The difference, however, resided in the substitution pattern of the cyclohexane ring. Key spin systems were established from the COSY spectrum, which revealed correlations between the two methine protons H-8 (δ_H 5.83) and H-9 (δ_H 6.79), between the methylene protons H_2-6 (δ_H 2.61/2.67) and the methine H-5 (δ_H 3.67), and between the methylene H_2-10 (δ_H 3.50/3.57) and the methyl group H_3-11 (δ_H 1.10) (Fig. 2). HMBC data further defined the substructure: cross-peaks from H-8 to both the hydroxyl-bearing carbon (δ 70.7) and the methylene carbon C-6 (δ_C 40.4), from H-9 to the oxygenated C-5 (δ_C 79.1) and the carbonyl C-7 (δ_C 197.1), from H_2-6 to the hydroxylated carbon C-4, and from H_3-11 to the methylene carbon C-10 (δ_C 64.8) established the planar structure as shown (Fig. 2). The proposed relative configuration of **4**, named melodamide C, was supported by a NOESY correlation between the C-5

Table 1
^{1}H and^{13}C NMR data for compounds **3** (in $CDCl_3$) and **4**–**5** (in DMSO-d_6).

3 ($CDCl_3$)			4 (DMSO-d_6)			5 (DMSO-d_6)		
position	δ_C, *type*	δ_H, *mult. (J in Hz)*	position	δ_C, *type*	δ_H, *mult. (J in Hz)*	position	δ_C, *type*	δ_H, *mult. (J in Hz)*
1-NH		6.18, brs	1-NH		8.15, t (5.5)	1-NH		8.16, t (5.5)
2	35.6, CH_2	3.62, q (6.0)	2	34.2, CH_2	3.37[a]	2	38.9, CH_2	3.33[a]
3	41.9, CH_2	1.84, t (6.0)	3a	37.7, CH_2	1.83, m	3	30.2, CH_2	2.64, m
			3b		1.90, m			
4	69.6, C		4	70.7, C		4	126.0, C	
5a	37.5, CH_2	2.10, m	5	79.1, CH	3.67, m	5	147.6, C	
5b		1.79, ddd (14.5, 13.2, 4.4)						
6a	37.1, CH_2	2.77, ddd (15.0, 14.0, 6.0)	6	40.4, CH_2	2.67, dd (16.9, 3.3)	6	115.4, CH	6.59, d (8.0)
6b		2.26, dt (15.0)			2.61, dd (16.9, 6.0)			
7	211.6, CO		7	197.1, CO		7	113.3, CH	6.43, dd (8.0, 2.0)
8a	37.1, CH_2	2.77, ddd (15.0, 14.0, 6.0)	8	127.7, CH	5.83, d (10.3)	8	149.6, C	
8b		2.26, dt (15.0)						
9a	37.5, CH_2	2.10, m	9	153.2, CH	6.79, d (10.3)	9	116.7, CH	6.48, d (2.0)
9b		1.79, ddd (14.5, 13.2, 4.4)						
			10a	64.8, CH_2	3.57, m			
			10b		3.50, m			
			11	15.5, CH_3	1.10, t (7.0)			
1′	166.9, CO		1′	164.8, CO		1′	164.8, CO	
2′	120.2, CH	6.38 d (15.5)	2′	122.2, CH	6.60 d (15.8)	2′	122.4, CH	6.62 d (15.5)
3′	142.1, CH	7.66, d (15.5)	3′	138.5, CH	7.39, m	3′	138.3, CH	7.42, d (15.5)
4′	135.1, C		4′	134.9, C		4′	134.9, C	
5′	128.0, CH	7.50, m	5′	127.5, CH	7.55, d (7.5)	5′	127.4, CH	7.56, brd (7.4)
6′	129.1, CH	7.39, m	6′	128.9, CH	7.41, m	6′	128.9, CH	7.42, m
7′	130.1, CH	7.38, m	7′	129.4, CH	7.38, m	7′	129.3, CH	7.39, m
8′	129.1, CH	7.39, m	8′	128.9, CH	7.41, m	8′	128.9, CH	7.42, m
9′	128.0, CH	7.50, m	9′	127.5, CH	7.55, d (7.5)	9′	127.4, CH	7.56, brd (7.4)
4-OH		–[a]			5.03, s			
5-OH								8.64, s
8-OH								8.56, s

[a] Overlapping signals.

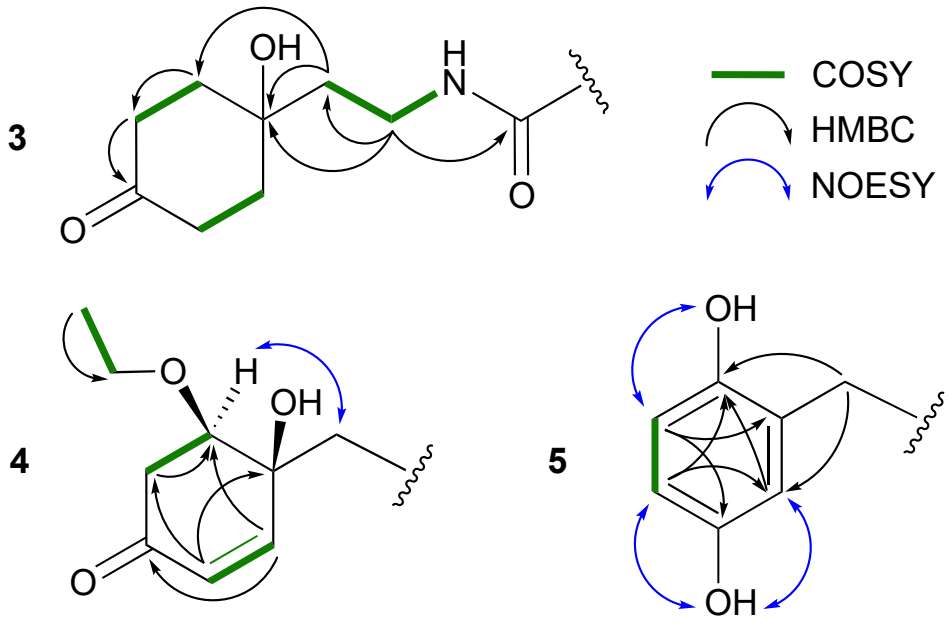

Fig. 2. Key COSY, HMBC and NOESY correlations of **3**–**5**.

methine and the C-3 methylene protons (Fig. 2 and S12).

Compound **5** gave the molecular formula $C_{17}H_{17}NO_3$, as indicated by HRESIMS showing an $[M + H]^+$ ion peak at *m/z* 284.1288 (calcd for $C_{17}H_{18}NO_3^+$ 284.1281) (Fig. S14). The NMR features of compound **5** were consistent with the presence of the *N*-ethylcinnamamide unit, identical to that of melodamides A-C. The aromatic region of the ^1H NMR spectrum (Fig. S16) also displayed an AMX spin system, with two ortho-coupled doublets at δ_H 6.59 (1H, d, $J = 8.0$ Hz, H-6) and 6.48 (1H, d, $J = 2.0$ Hz, H-9), together with a doublet of doublets at δ_H 6.43 (1H, dd, $J = 8.0$, 2.0 Hz, H-7). This coupling pattern was indicative of a trisubstituted benzene ring *para*-substituted with two hydroxy groups. Their position was established by the HMBC data showing cross-peaks from the methylene protons H_2-3 (δ_H 2.64) to the protonated aromatic carbon C-9 (δ_C 116.7) and the oxygenated carbon C-5 (δ_C 147.6), from H-6 (δ_H 6.59) to the quaternary aromatic carbon C-4 (δ_C 126.0) and the oxygenated carbon C-8 (δ_C 149.6), from H-7 (δ_H 6.43) to C-5 and C-9, and from H-9 (δ_H 6.48) to C-5 (Fig. S19). Additional support for this substitution pattern came from NOE correlations, specifically between OH-5 (δ_H 8.64) and H-6, and between OH-8 (δ_H 8.56) and both H-7 and H-9 (Fig. S20). On this basis, the structure of compound **5** was assigned and designated as melodamide D.

Compounds **6**–**11** were identified as uvariadiamide (**6**) (Yang et al., 2010), 2′,4′-dihydroxy-4,6′-dimethoxychalcone (**7**) (Thuy et al., 1998; Seidel et al., 2000), alpinetin (**8**) (Phan et al., 2005; Xiao et al., 2011), 7, 4′-dihydroxy-5-methoxyflavanone (**9**) (Phan et al., 2005), melosiamensone B (**10**) (Jaidee et al., 2019), and tsugafolin (**11**) (Seidel et al., 2000) by comparison of their spectroscopic data with those reported in the literature.

2.2. Biological assays

The successive fractionation steps and associated antiviral activities that guided the isolation process are summarized in the Supporting Information (Fig. S22). The antiviral activity of the isolated compounds (**1**–**11**) was evaluated against HCoV-229E using Huh-7 cells infected at a multiplicity of infection (MOI) of 0.1 for 24 h. Cell viability (CC_{50}) was determined in parallel after 48 h of compound exposure to assess cytotoxicity under identical conditions. Remdesivir was included as an

Table 2
Antiviral and cytotoxic activities of compounds **1**–**11**.

Compound	Huh7	HCoV-229E	SI	Vero E6	SARS-CoV-2	SI
	CC_{50}	IC_{50}		CC_{50}	IC_{50}	
(+)**1**	60.5 ± 15.5	1.4 ± 0.6	43.2	191.5 ± 18.6	32.1 ± 0.5	6.0
(−)**1**	76.5 ± 14.2	9.9 ± 2.3	7.8	144.5 ± 16.5	31.7 ± 1.6	4.6
(±)**1** (racemate)	71.2 ± 7.6	1.8 ± 0.4	39.3	125.0 ± 11.5	25.4 ± 3.7	4.9
2	47.1 ± 5.9	4.2 ± 2.5	11.3	120.5 ± 18.3	40.1 ± 8.6	3.0
3	>200	na	-	>200	na	-
4	71.0 ± 11.7	1.8 ± 0.01	39.2	152.0 ± 22.6	48.3 ± 3.8	3.2
5	115.5 ± 7.5	18.8 ± 4.5	6.2	>200	74.2 ± 9.7	2.7
6	>200	71.6 ± 21.5	2.8	>200	na	-
7	108.0 ± 12.2	11.0 ± 6.4	9.8	>200	36.1 ± 8.5	5.5
8	>200	38.8 ± 8.5	5.2	>200	na	-
9	>200	86.7 ± 5.7	2.3	>200	na	-
10	151.0 ± 14.1	8.4 ± 0.1	17.9	>200	na	-
11	>200	8.4 ± 0.2	23.8	>200	na	-
Remdesivir	95.0 ± 2.5	0.1 ± 0.05	950.0	>200	25 ± 3.8	8.0

Cytotoxic concentration (CC_{50}) and inhibitory concentration (IC_{50}) values were determined by nonlinear regression followed by the construction of sigmoidal concentration–response curves. CC_{50} and IC_{50} values are expressed in μM as mean ± SD from three independent biological experiments, each performed in technical triplicate. The Selectivity Index (SI) was calculated as CC_{50}/IC_{50}. "na" indicates not active, i.e., no reliable IC_{50} value could be determined at the highest non-cytotoxic concentration tested.

internal positive control (Table 2).

The bioassay-guided fractionation of *U. siamensis* extracts led to the identification of two main families of metabolites, amide derivatives (**1**–**6**) and polyphenols (**7**–**11**), showing distinct antiviral profiles (Table 2). Among the amide derivatives, (+)-toussaintine C (**1**) emerged as the most potent compound, with an IC_{50} of 1.4 μM and a SI of 43.2, reflecting both strong antiviral potency and limited cytotoxicity (Table 2). Its enantiomer (−)-toussaintine C was markedly less active (IC_{50} = 9.9 μM, SI = 7.8), highlighting a clear stereochemical dependence of antiviral activity against HCoV-229E. Melodamide C (**4**) also displayed strong antiviral activity (IC_{50} = 1.8 μM, SI = 39.2), comparable to (+)-toussaintine C, whereas melodamide A (**2**) also showed clear antiviral activity (IC_{50} = 4.2 μM, SI = 11.3). In contrast, melodamides B (**3**), D (**5**), and uvariadiamide (**6**) were weakly active or inactive.

The limited number of analogues and the variability in biological responses preclude definitive structure-activity relationship conclusions. Within the melodamide series, all compounds share the same *N*-ethylcinnamamide unit, and variations in activity arise from modifications of the cyclohexanone-derived moiety, without revealing a clear linear trend. Compounds **2** and **4** exhibited antiviral activity within the same order of magnitude, while other structurally related analogues were weakly active or inactive. Although melodamide D (**5**), which features an aromatic ring, showed reduced activity, no conclusion can be drawn regarding the influence of aromaticity, as other weakly active analogues, such as melodamide B (**3**), do not contain an aromatic moiety. Toussaintine C also displayed antiviral activity within a similar range, indicating that both scaffolds can support activity. In contrast, a significant difference was observed between the enantiomers of toussaintine C, with (+)-**1** being markedly more active than (−)-**1**, suggesting that stereochemistry may play a role in antiviral activity.

The polyphenolic derivatives (**7**–**11**) exhibited variable and generally moderate activity against HCoV-229E, with IC_{50} values ranging from 8.4 to 86.7 μM and selectivity indices between 2.3 and 23.8. Although less potent than the amide derivatives, these results suggest that certain hydroxylated flavonoids or chalcone-like frameworks may contribute to residual antiviral activity observed in the crude extracts. Overall, the amide series (**1**–**6**) demonstrated higher potency and selectivity than the polyphenols, confirming that these cinnamamide derivatives constitute the primary antiviral structural class within *U. siamensis*.

The compounds were also evaluated for antiviral activity against the pandemic clinical isolate SARS-CoV-2 in Vero E6 cells infected at MOI of 0.1 for 48 h, after assessing their cytotoxicity under identical culture conditions. As observed for HCoV-229E, all forms of toussaintine C, (+), (−), and racemic, displayed comparable inhibitory activity profile against SARS-CoV-2, with IC_{50} values ranging from 25.4 to 32.1 μM. The (+) enantiomer showed the highest selectivity index (SI = 6.0), although the difference with the (−) enantiomer and the racemic mixture (SI = 4.6 and 4.9, respectively) remained modest. Melodamides A (**2**) and C (**4**) exhibited moderate inhibitory activity (IC_{50} = 40.1 and 48.3 μM, respectively), whereas the remaining amides were inactive or weakly active. Most polyphenolic compounds were inactive against SARS-CoV-2, with the exception of compound **7**, which retained moderate inhibition (IC_{50} = 36.1 μM).

These observations indicate that the amide derivatives identified from *U. siamensis* display stronger apparent activity in the HCoV-229E/Huh-7 model than in the SARS-CoV-2/Vero E6 model. However, this difference should be interpreted cautiously, because the assays compare two distinct virus-cell systems rather than the two viruses under identical experimental conditions. HCoV-229E uses human aminopeptidase N/CD13, rather than ACE2, as its main entry receptor, and its Spike protein can be activated through TMPRSS2- or cathepsin-dependent pathways (Yeager et al., 1992; Bertram et al., 2013). SARS-CoV-2, in contrast, relies on ACE2 binding and Spike priming by host proteases such as TMPRSS2, although the preferred entry route depends on the cellular context (Hoffmann et al., 2020; Pires de Souza et al., 2022). This is particularly relevant here because Vero E6 cells are highly permissive to SARS-CoV-2 and are associated with high ACE2 but low TMPRSS2 expression, whereas Huh-7 cells strongly express TMPRSS2 but show low or undetectable ACE2 expression and support only moderate SARS-CoV-2 replication (Pires de Souza et al., 2022). Thus, the different activity profiles may reflect not only viral differences, but also receptor/protease usage, replication efficiency, host-cell permissiveness, compound handling by the cells, and assay format. Comparative assays in matched cellular models, together with time-of-addition, entry, and post-entry replication assays, will be required to clarify the mechanism of action.

To qualitatively confirm the antiviral activities observed in the quantitative assays, we next evaluated the four compounds that showed activity against both HCoV-229E and SARS-CoV-2, (+)- and (−)-toussaintine C (**1**), melodamide A (**2**), and melodamide C (**4**), using an independent immunofluorescence assay (Fig. 3). Vero E6 cells were infected with SARS-CoV-2 (MOI 0.1) and treated for 48 h at 50, 25, and 12.5 μM, concentrations bracketing the previously determined IC_{50} values. Nirmatrelvir was included as a positive control. Staining of the viral Spike protein revealed a clear dose-dependent reduction of infected cells for all four compounds.

At 50 μM, both enantiomers of toussaintine C (**1**) and melodamide C (**4**) markedly suppressed viral antigen expression, whereas partial inhibition was still observed at 25 μM and more visibly at 12.5 μM. Melodamide A (**2**) showed a similar but slightly weaker effect, consistent with its lower potency in the primary assay (Fig. 3). Altogether, these imaging data corroborate the antiviral effects quantified in the screening assays and confirm that these cinnamamide derivatives exert genuine inhibitory activity against SARS-CoV-2 in infected cells.

3. Conclusions

The bioassay-guided investigation of *U. siamensis* led to the identification of amide derivatives with significant antiviral activity. Although compounds **3**–**5** share the *N*-ethylcinnamamide moiety with melodamide A, they differ in the nature of the cyclohexanone moiety replacing the *p*-quinol unit, resulting in distinct oxidation states and structural features that expand the structural diversity within this class of cinnamamide derivatives. (+)-Toussaintine C and melodamides A and C displayed the most pronounced inhibitory effects against HCoV-229E and retained moderate activity against SARS-CoV-2, as confirmed by immunofluorescence assays. These findings highlight *U. siamensis* as a source of cinnamamide derivatives with antiviral potential, with potent activity in the HCoV-229E model and measurable cross-coronavirus activity against SARS-CoV-2. Future studies should aim to define the affected step of the viral life cycle, assess selectivity toward viral and host targets, evaluate chemical and metabolic stability, and confirm activity in more physiologically relevant respiratory models. Overall, these results identify natural cinnamamide derivatives as useful starting points for further coronavirus inhibitor discovery.

4. Experimental

4.1. General experimental procedures

Optical rotations were measured at 20 °C on an Anton Paar MCP 300 polarimeter. NMR spectra of compounds **3**–**5** were recorded on Bruker 700 (compound **4**), 500 (compound **3**) and 300 (compound **5**) MHz instruments (Avance 500 and 300). Chemical shifts, relative to $CDCl_3$ (compound **3**) or DMSO-d_6 (compounds **4**–**5**), are in ppm and coupling constants are in Hz. Nucleodur analytical, semi-preparative and preparative C_{18} and PFP columns (250 × 4.6 mm, 250 × 10 mm and 250 × 20 mm; 5 μm, Macherey-Nagel) were used for HPLC separations using a Waters autopurification system equipped with a sample manager (Waters 2767), a column fluidics organizer, a binary pump (Waters

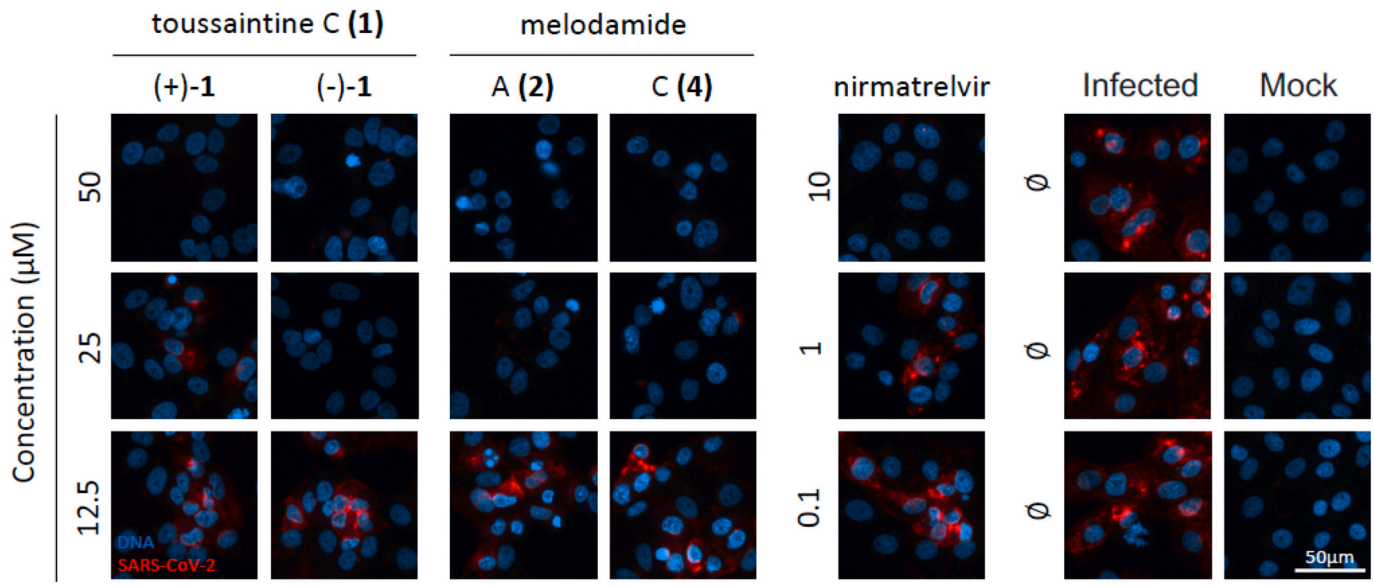

Fig. 3. Qualitative immunofluorescence analysis of SARS-CoV-2 infection in Vero E6 cells treated with compounds 1, 2, and 4, identified as active against both HCoV-229E and SARS-CoV-2. Vero cells were infected (MOI 0.1) and treated for 48 h at 50, 25, and 12.5 μM. Nirmatrelvir (10, 1, 0.1 μM) was included as a reference inhibitor. Controls correspond to infected cells treated with vehicle (Infected) and to non-infected cells (Mock). Nuclei were stained with DAPI, and SARS-CoV-2 antigen was detected using an anti-Spike antibody. Scale bar: 50 μm.

2525), a UV–vis diode array detector (190–600 nm, Waters 2996), and a PL-ELS 1000 ELSD Polymer Laboratory detector. HRESIMS data were acquired using an Acquity Waters UPLC coupled to a Waters LCT Premier XE mass spectrometer. The ionization was carried out using an electrospray ionization source in the positive mode (range *m/z* 80−1500). All solvents were purchased from Carlo Erba (France) or SDS (Peypin, France) and analytical TLC plates (Si gel 60 F254) were from Merck (France). Prepacked Flash Pur EcoFlex Büchi (France) silica gel (50 μm, irregular) cartridge was used for flash chromatography using a Teledyne Isco Combiflash Rf 200i.

4.2. Plant material

Leaves of *Uvaria siamensis* (Scheff.) L.L.Zhou, Y·C·F.Su & R.M.K. Saunders were collected in June 2007 in Sơ Pai, K'Bang, Gia Lai, Vietnam. The plant material was initially identified as *Melodorum fruticosum* by Dr. Nguyen The Cuong. Following the taxonomic revision of Turner (2018), in which *Melodorum fruticosum* is treated as a synonym of *Uvaria siamensis*, the accepted name *U. siamensis* was adopted in the present study. A voucher specimen (VN-1815) has been deposited at the Herbarium of the Institute of Biology, Vietnam Academy of Science and Technology (VAST), Hanoi, and is available for consultation.

Leaves were dried at a temperature not exceeding 40 °C using a hot air generator before being ground and stored at room temperature.

4.3. Extraction and isolation

Ground leaves (0.86 kg) of *U. siamensis* were extracted successively with EtOAc (3 x 2 L, 1 h each, 40 °C) and MeOH (2 x 2 L, 1 h each, 40 °C). Concentration *in vacuo* afforded 6.6 g (EtOAc) and 16.5 g (MeOH) of crude extracts.

The EtOAc extract was subjected to silica gel flash chromatography (220 g) using a gradient of *n*-heptane/EtOAc/MeOH with increasing polarity (100:0:0 to 0:100:0 in 80 min to 0:80:20 in 40 min, 75 mL min^{-1}) to afford 22 fractions, F1–F22, according to their TLC profiles. F9 yielded pure compound **7** (306 mg). F12 (150.0 mg) was purified by preparative HPLC (Nucleodur C_{18}, H_2O–CH_3CN + 0.1% formic acid, 65:35 at 21 mL min^{-1}) to afford compound **5** (11.9 mg, t_R 13.3 min) and **8** (22.6 mg, t_R 23.9 min). F16 (150 mg) was purified by preparative HPLC (Nucleodur C_{18}, H_2O–CH_3CN + 0.1% formic acid, 70:30 at 21 mL min^{-1}) to yield compound **2** (76.8 mg, t_R 10.6 min) and **6** (4.6 mg, t_R 19.3 min). F17 (700.0 mg) was further purified by flash chromatography over silica gel (4 g) using a gradient of *n*-heptane/EtOAc (100:0 to 0:100, 130 min), followed by an EtOAc/MeOH rinse 80:20 for 20 min, 12 mL min^{-1}) to give a racemic mixture of **1** (98.5 mg, t_R 44.0 min). Compound **1** (10.0 mg) was then subjected to semi-preparative chiral HPLC (CHIRALPAK® ID, *n*-heptane-EtOH, 50:50 at 3 mL min^{-1}), affording compounds (+)-**1** (2.8 mg, t_R 11.0 min) and (−)-**1** (2.4 mg, t_R 17.0 min). F18 was purified by semi-preparative HPLC (Nucleodur PFP, H_2O–CH_3CN + 0.1% formic acid, 65:35 for 5 min to 15:85 in 30 min at 4.7 mL min^{-1}) to afford sub-fraction 4 (10.0 mg, t_R 7.5 min). Sub-fraction 4 was further purified by preparative HPLC (Nucleodur C_{18}, H_2O–CH_3OH, 60:40 at 21 mL min^{-1}) to yield compound **3** (1.3 mg, t_R 44.0 min).

The MeOH extract (16.5 g) was subjected to silica gel flash chromatography (330 g silica gel) using a gradient of *n*-heptane/EtOAc (100:0 to 0:100) in 180 min, 100 mL min^{-1}) to afford 23 fractions, F1–F23, according to their TLC profiles. F14 (557.0 mg) was purified by preparative HPLC (Nucleodur C_{18}, H_2O–CH_3CN + 0.1% formic acid, 70:30 to 0:100 in 30 min at 21 mL min^{-1}) to afford compound **9** (7.0 mg, t_R 8.4 min), compound **2** (350.0 mg, t_R 10.5 min), compound **4** (14.0 mg, t_R 16.6 min), compound **6** (36.0 mg, t_R 17.5 min), compound **10** (2.6 mg, t_R 22 min) and **11** (5.2 mg, t_R 24.4 min). F15 and F16 were combined (907 mg) and further purified by silica gel flash chromatography (40 g silica gel, *n*-heptane/EtOAc (100:0 to 0:100) in 30 min, 18 mL min^{-1}) to afford the racemate of toussaintine C (225 mg).

4.4. Spectroscopic data

4.4.1. Melodamide B (3)

Yellow amorphous solid; ^1H and ^{13}C NMR, see Table 1; HRESIMS *m/z* 288.1592 $[M+H]^+$ (calcd for $C_{17}H_{22}NO_3^+$ 288.1594). UV λ_{max} (log ε) 274 (4.12), 216 (4.03) nm (MeOH), IR ν_{max} 3318, 2926, 1707, 1656, 1615, 1547, 1449, 1343, 1224, 1130, 977, 766 cm^{-1}, NP-MRD ID: NP0351872.

4.4.2. Melodamide C (4)

White amorphous solid; $[\alpha]_D^{25}$ −8.7° (*c* 0.1, MeOH); ^1H and ^{13}C NMR,

see Table 1; HRESIMS *m/z* 330.1710 $[M+H]^+$ (calcd for $C_{19}H_{24}NO_4^+$ 330.1700). UV λ_{max} (log ε) 277 (4.23), 222 (4.43) nm (MeOH), IR ν_{max} 3288, 3063, 2934, 2827, 1640, 1626, 1578, 1546, 1497, 1450, 1394, 1342, 1302, 1284, 1224, 1169, 1093, 979, 918, 862, 767, 705, 685 cm^{-1}, NP-MRD ID: NP0351873.

4.4.3. Melodamide D (5)

Yellow amorphous solid; ^1H and ^{13}C NMR, see Table 1; HRESIMS *m/z* 284.1288 $[M+H]^+$ (calcd for $C_{17}H_{18}NO_3^+$ 284.1281). UV λ_{max} (log ε) 277 (4.37), 216 (4.33), 206 (4.33) nm (MeOH), IR ν_{max} 3336, 2920, 1661, 1609, 1555, 1457, 1368, 1207, 978, 770 cm^{-1}, NP-MRD ID: NP0351874.

4.5. Biological assays

4.5.1. Cells, viruses and reagents

Huh-7 human hepatoma cells (ATCC PTA-8561) and Vero E6 kidney epithelial cells (ATCC CCL-81) were maintained in Dulbecco's Modified Eagle Medium (DMEM) supplemented with 10% fetal bovine serum (FBS). The culture medium was further enriched with 2 mM L-glutamine, 1 mM sodium pyruvate, and standard antimicrobial additives consisting of 100 $U.mL^{-1}$ penicillin, 0.1 mg mL^{-1} streptomycin, and 0.5 µg mL^{-1} fungizone. Cells were grown at 37 °C in a humidified incubator with 5% CO_2.

The recombinant luciferase-expressing Human Coronavirus 229E (HCoV-229E-Luc) used in this work was kindly provided by van den Worm and Eriksson. The SARS-CoV-2 strain employed for infection assays originated from a nasopharyngeal swab collected in Réunion Island in 2020 from a PCR-confirmed COVID-19 case. Viral stocks for SARS-CoV-2 were amplified in Vero E6 cells, whereas HCoV-229E-Luc propagation was performed in Huh-7 cells. Remdesivir was obtained from Invivogen (Toulouse, France). Nirmatrelvir (PF-07321332) was sourced from Merck (France). All compounds were solubilized in sterile dimethyl sulfoxide (DMSO; Sigma-Aldrich) to prepare stock solutions. The monoclonal anti-SARS-CoV-2 Spike antibody (human IgG1, clone H4) was sourced from Invivogen.

4.5.2. Mitochondrial activity assay

Cytotoxicity of the purified compounds was assessed using an MTS-based colorimetric assay (CellTiter Aqueous One Solution Cell Proliferation Assay, Promega). Huh-7 or Vero E6 cells were seeded in 96-well plates at a density of 2×10^4 cells per well and allowed to adhere before being exposed to serial dilutions of each compound. After a 48-h incubation period, cell metabolic activity was quantified according to the manufacturer's instructions by adding the MTS reagent directly to the wells. Absorbance was recorded at 490 nm, and cell viability was expressed as a percentage relative to untreated controls. Concentration–response curves were fitted using GraphPad Prism, from which the 50% cytotoxic concentration (CC_{50}) values were calculated from three independent biological assays performed in triplicate.

4.5.3. Antiviral assay (HCoV-229E and SARS-CoV-2)

The antiviral properties of compounds were first examined using a recombinant HCoV-229E strain expressing a luciferase reporter (HCoV-229E-Luc). Huh-7 cells were seeded in 96-well plates and infected at a multiplicity of infection (MOI) of 0.1 in a final volume of 50 µL, together with serial dilutions of the test samples. After a 24 h incubation at 37 °C, cells were lysed by adding 20 µL of Renilla luciferase lysis buffer (Promega, E2810), and luminescence was measured on a FLUOstar Omega reader using the Renilla luciferase detection system according to the manufacturer's recommendations. Viral inhibition was expressed relative to DMSO-treated infected controls, and IC_{50} values were determined from dose–response curves.

For SARS-CoV-2, antiviral activity was assessed by flow cytometry. Vero E6 cells were plated in 96-well plates, allowed to adhere overnight, and then exposed to SARS-CoV-2 at an MOI of 0.1 in the presence of increasing concentrations of the purified phytochemicals for 48 h at 37 °C. At the end of the incubation period, cells were detached using trypsin, fixed for 20 min in 3.7% formaldehyde, and washed with PBS. Intracellular viral antigen was detected by staining with a human IgG1 monoclonal antibody targeting the SARS-CoV-2 Spike protein (clone H4), followed by an Alexa Fluor 488-conjugated goat anti-human IgG secondary antibody. Samples were analyzed on a CytoFLEX cytometer (Beckman Coulter), and the proportion of Spike-positive cells was quantified using CytExpert software. IC_{50} values were calculated from the percentage of infected cells relative to untreated controls.

4.5.4. Immunofluorescence assay

Immunofluorescence analyses were carried out on Vero E6 cells following infection and compound treatment. Cells were first fixed in 4% paraformaldehyde prepared in PBS for 15 min at room temperature, then washed three times with PBS. Permeabilization and blocking were performed for 45 min in PBS supplemented with 2% BSA and 0.1% Triton X-100. Cells were subsequently incubated for 2 h at room temperature with a primary antibody directed against the SARS-CoV-2 Spike protein, diluted in PBS containing 0.5% BSA and 0.05% Triton X-100. After three washes of 5 min each in PBS, samples were incubated for 1 h with an Alexa Fluor 594–conjugated anti-human IgG secondary antibody (Invitrogen, 1:750) together with DAPI for nuclear staining, using the same dilution buffer. Cells were then washed three additional times and imaged using a Zeiss Celldiscoverer 7 microscope equipped with a 20×/0.7 NA objective and a 0.5× tube lens.

CRediT authorship contribution statement

Bastien Petit: Formal analysis, Investigation. **Thibaud Goupil:** Formal analysis. **Linh Hoang Phan:** Formal analysis. **Charline Herrscher:** Formal analysis. **Thomas Gaslonde:** Formal analysis. **Xavier Cachet:** Formal analysis. **Van Cuong Pham:** Investigation, Resources. **Thi Mai Huong Doan:** Investigation, Resources. **Karin Séron:** Formal analysis, Methodology, Validation. **Fanny Roussi:** Validation. **Sandy Desrat:** Validation. **Marc Litaudon:** Conceptualization, Funding acquisition, Methodology, Project administration, Validation, Writing – review & editing. **Chaker El Kalamouni:** Conceptualization, Funding acquisition, Methodology, Project administration, Supervision, Validation, Writing – original draft. **Cécile Apel:** Conceptualization, Methodology, Project administration, Supervision, Validation, Visualization, Writing – original draft, Writing – review & editing.

Declaration of competing interest

The authors declare that they have no known competing financial interests or personal relationships that could have appeared to influence the work reported in this paper.

Acknowledgments

We gratefully acknowledge the International Associated Laboratory (LIA: NATPROCHEMLAB) between the Centre National de la Recherche Scientifique (CNRS, ICSN, France) and the Vietnam Academy of Science and Technology (Institute of Chemistry, VAST, Vietnam). This work received financial support from the Université Paris-Saclay and the Agence Nationale pour la Recherche (ANR-11-IDEX-0003-02 (10-LABX-0033), from the POE FEDER 2014-20 of the Conseil Régional de La Réunion (TFORCE-COVIR, N°20201437-0027601) and from the PHYTODENGUE program (N° SYNERGIE: RE0028005). We express our appreciation to Nathan François and Sandrine Belouzard of the Center for Infection and Immunity of Lille (CIIL) for their preliminary assessments regarding the antiviral properties of plant extracts against HCoV-229E. This work was performed using the infrastructure and technical support of the Department of Collections, Scientific Platforms and Services at ICSN.

Appendix A. Supplementary data

Supplementary data to this article can be found online at https://doi.org/10.1016/j.phytochem.2026.115010.

Data availability

No data was used for the research described in the article.

References

Apel, C., Haddad, J., Herrscher, C., Grisel, C., Girard, J., Olivon, F., Poullain, C., Gallard, J.-F., Boutet, S., Roussi, F., Desrat, S., El Kalamouni, C., Litaudon, M., 2025. Comptonellins A–H, highly potent antiviral ternatin-type cyclopeptides from *Comptonella drupacea*. J. Nat. Prod. 88 (6), 1399–1412. https://doi.org/10.1021/acs.jnatprod.5c00318.

Bertram, S., Dijkman, R., Habjan, M., Heurich, A., Gierer, S., Glowacka, I., Welsch, K., Winkler, M., Schneider, H., Hofmann-Winkler, H., Thiel, V., Pöhlmann, S., 2013. TMPRSS2 activates the human coronavirus 229E for cathepsin-independent host cell entry and is expressed in viral target cells in the respiratory epithelium. J. Virol. 87, 6150–6160. https://doi.org/10.1128/JVI.03372-12.

Chambon, M., Herrscher, C., Al Halabi, D., François, N., Belouzard, S., Boutet, S., Pham, V.C., Doan, T.M.H., Séron, K., Mavingui, P., Litaudon, M., El Kalamouni, C., Apel, C., 2023. New phenolic lipids from the leaves of *Clausena harmandiana* inhibit SARS-CoV-2 entry into host cells. Molecules 28 (14), 5414. https://doi.org/10.3390/molecules28145414.

Chan, H.-H., Hwang, T.-L., Thang, T.D., Leu, Y.-L., Kuo, P.-C., Nguyet, B.T.M., Dai, D.N., Wu, T.-S., 2013. Isolation and synthesis of melodamide A, a new anti-inflammatory phenolic amide from the leaves of *Melodorum fruticosum*. Planta Med. 79, 288–294. https://doi.org/10.1055/s-0032-1328131.

de Wit, E., van Doremalen, N., Falzarano, D., Munster, V.J., 2016. SARS and MERS: recent insights into emerging coronaviruses. Nat. Rev. Microbiol. 14 (8), 523–534. https://doi.org/10.1038/nrmicro.2016.81.

Do, L.T.M., Sichaem, J., 2022. New flavonoid derivatives from *Melodorum fruticosum* and their α-Glucosidase inhibitory and cytotoxic activities. Molecules 27 (13), 4023. https://doi.org/10.3390/molecules27134023.

Hoffmann, M., Kleine-Weber, H., Schroeder, S., Krüger, N., Herrler, T., Erichsen, S., Schiergens, T.S., Herrler, G., Wu, N.H., Nitsche, A., Müller, M.A., Drosten, C., Pöhlmann, S., 2020. SARS-CoV-2 cell entry depends on ACE2 and TMPRSS2 and is blocked by a clinically proven protease inhibitor. Cell 181, 271–280.e8. https://doi.org/10.1016/j.cell.2020.02.052.

Jaidee, W., Andersen, R.J., Chavez, M.A.G., Wang, Y.A., Patrick, B.O., Pyne, S.G., Muanprasat, C., Borwornpinyo, S., Laphookhieo, S., 2019. Amides and flavonoids from the fruit and leaf extracts of *Melodorum siamensis*. J. Nat. Prod. 82 (2), 283–292. https://doi.org/10.1021/acs.jnatprod.8b00696.

Jung, J.H., Chang, C.-J., Smith, D.L., McLaughlin, J.L., 1991. Additional bioactive heptenes from *Melodorum fruticosum*. J. Nat. Prod. 54 (2), 500–505. https://doi.org/10.1021/np50074a023.

Jung, J.H., Pummangura, S., Chaichantipyuth, C., Patarapanich, C., Fanwick, P.E., Chang, C.-J., Mclaughlin, J.L., 1990. New bioactive heptenes from *Melodorum fruticosum* (Annonaceae). Tetrahedron 46 (15), 5043–5054. https://doi.org/10.1016/S0040-4020(01)87811-X.

Kronenberger, T., Laufer, S.A., Pillaiyar, T., 2023. COVID-19 therapeutics: small-molecule drug development targeting SARS-CoV-2 main protease. Drug Discov. Today 28 (6), 103579. https://doi.org/10.1016/j.drudis.2023.103579.

Nguyen, H.T.M., Ngo, D.T.T., Nguyen, P.D.N., Pham, T.N.K., Do, L.T.M., Sichaem, J., 2024. New prenyl flavanone and diarylbutanol from *Uvaria siamensis* stem bark and their α-Glucosidase inhibitory activity. Nat. Prod. Res. 38 (22), 3982–3988. https://doi.org/10.1080/14786419.2023.2272024.

Petit, B., Marguerite, E., Van Elslande, E., Nedev, H., Iorga, B.I., Pham, V.C., Doan, T.M.H., Séron, K., Litaudon, M., El Kalamouni, C., Apel, C., 2024. Antiviral miliusanes and isolation of an unprecedented miliusane dimer from *Miliusa balansae*. Fitoterapia 177, 106083. https://doi.org/10.1016/j.fitote.2024.106083.

Phan, M.G., Dang, B.T., Phan, T.S., 2005. Flavonoid compounds from the rhizomes of *Alpinia conchigera* griff. Zingiberaceae. Vietnam J. Chem. 43 (1), 105–108.

Pires de Souza, G.A., Le Bideau, M., Boschi, C., Wurtz, N., Colson, P., Aherfi, S., Devaux, C., La Scola, B., 2022. Choosing a cellular model to study SARS-CoV-2. Front. Cell. Infect. Microbiol. 12, 1003608. https://doi.org/10.3389/fcimb.2022.1003608.

Pripdeevech, P., Chukeatirote, E., 2010. Chemical compositions, antifungal and antioxidant activities of essential oil and various extracts of *Melodorum fruticosum* L. flowers. Food Chem. Toxicol. 48 (10), 2754–2758. https://doi.org/10.1016/j.fct.2010.07.002.

Salae, A.-W., Chairerk, O., Sukkoet, P., Chairat, T., Prawat, U., Tuntiwachwuttikul, P., Chalermglin, P., Ruchirawat, S., 2017. Antiplasmodial dimeric chalcone derivatives from the roots of *Uvaria siamensis*. Phytochemistry 135, 135–143. https://doi.org/10.1016/j.phytochem.2016.12.009.

Samwel, S., Odalo, J.O., Nkunya, M.H.H., Joseph, C.C., Koorbanally, N.A., 2011. Toussaintines A–E: antimicrobial indolidinoids, a cinnamoylhydrobenzofuranoid and a cinnamoylcyclohexenoid from *Toussaintia orientalis* leaves. Phytochemistry 72 (14), 1826–1832. https://doi.org/10.1016/j.phytochem.2011.05.010.

Schevenels, F.T., Jadsadajerm, S., Lekphrom, R., Yodsin, N., Suebrasri, T., Senawong, T., Wisetsai, A., 2025. Siamfuranones A–C, three novel furanone derivatives from the flowers of *Uvaria siamensis* and their biological activities. Nat. Prod. Res. 39 (14), 3930–3939. https://doi.org/10.1080/14786419.2024.2324370.

Seidel, V., Bailleul, F., Waterman, P.G., 2000. (*Rel*)-1β,2α-Di-(2,4-Dihydroxy-6-Methoxybenzoyl)-3β, 4α-Di-(4-Methoxyphenyl)-Cyclobutane and other flavonoids from the aerial parts of *Goniothalamus gardneri* and *Goniothalamus thwaitesii*. Phytochemistry 55 (5), 439–446. https://doi.org/10.1016/S0031-9422(00)00346-0.

Sukumaran, S.Y., Herrscher, C., Rasol, N.E., Othman, M.A., Liew, S.Y., Ismail, N.H., Séron, K., Litaudon, M., Awang, K., El Kalamouni, C., Apel, C., Zahari, A., 2024. Targeted isolation of antiviral labdane diterpenes from the bark of *Neo-uvaria foetida* (annonaceae) using LC-MS/MS-Based molecular networking. J. Nat. Prod. 87 (8), 1941–1951. https://doi.org/10.1021/acs.jnatprod.4c00342.

Tabtimmai, L., Choowongkomon, K., Kittakoop, P., Lekphrom, R., Schevenels, F.T., Jadsadajerm, S., Wisetsai, A., 2025. Lanostane triterpenes, flavanones and acetogenins from the roots of *Uvaria siamensis* and their cytotoxic activity. ACS Omega 10 (2), 2253–2259. https://doi.org/10.1021/acsomega.4c09267.

Takashima, K., Manse, Y., Suzuki, R., Masuda, N., Fukuda, Y., Fukuda, R., Marumoto, S., Ishikawa, F., Morikawa, T., Tanabe, G., 2025. Synthesis and biological evaluation of γ-Alkylidenebutenolides isolated from *Melodorum fruticosum*: the role of the Propylidene-Type side chain structure on anti-melanogenic activity. Org. Biomol. Chem. 23 (18), 4497–4507. https://doi.org/10.1039/D5OB00449G.

Thuy, T.T., Porzel, A., Ripperger, H., Sung, T.V., Adam, G., 1998. Chalcones and ecdysteroids from *Vitex leptobotrys*. Phytochemistry 49 (8), 2603–2605. https://doi.org/10.1016/S0031-9422(98)00411-7.

Turner, I.M., 2018. Annonaceae of the Asia-Pacific Region: names, types and distributions. Gard. Bull. Singap. 70 (2), 409–744. https://doi.org/10.26492/gbs70(2).2018-11.

Xiao, X., Si, X., Tong, X., Li, G., 2011. Preparation of flavonoids and diarylheptanoid from *Alpinia katsumadai hayata* by microwave-assisted extraction and high-speed counter-current chromatography. Sep. Purif. Technol. 81 (3), 265–269. https://doi.org/10.1016/j.seppur.2011.07.013.

Yang, X.-N., Jin, Y.-S., Zhu, P., Chen, H.-S., 2010. Amides from *Uvaria microcarpa*. Chem. Nat. Compd. 46 (2), 324–326. https://doi.org/10.1007/s10600-010-9605-6.

Yeager, C.L., Ashmun, R.A., Williams, R.K., Cardellichio, C.B., Shapiro, L.H., Look, A.T., Holmes, K.V., 1992. Human aminopeptidase N is a receptor for human coronavirus 229E. Nature 357, 420–422. https://doi.org/10.1038/357420a0.

Zhou, B., Gong, Q., Fu, Y., Zhou, J.-S., Zhang, H.-Y., Yue, J.-M., 2023. Sarglamides A–E, Indolidinoid–Monoterpenoid hybrids with anti-neuroinflammatory activity from a *sarcandra* species. Org. Lett. 25 (9), 1464–1469. https://doi.org/10.1021/acs.orglett.3c00196.

Zhou, L., Su, Y.C.F., Saunders, R.M.K., 2009. Molecular phylogenetic support for a broader delimitation of *uvaria* (Annonaceae), inclusive of *Anomianthus, Cyathostemma, Ellipeia, Ellipeiopsis* and *Rauwenhoffia*. Syst. Biodivers. 7 (3), 249–258. https://doi.org/10.1017/S1477200009003028.